Needle Heating During Interventional Magnetic Resonance Imaging at 1.5- and 3.0-T Field Strengths

Iman Khodarahmi, MD, PhD, Luke W. Bonham, BS,† Clifford R. Weiss, MD,† and Jan Fritz, MD, PD, DABR, RMSK**

Objectives: The aim of this study was to test the hypothesis that clinically used magnetic resonance (MR)–conditional needles of varying lengths, orientations, locations, and pulse sequences can result in excessive heating during MR imaging (MRI)–guided interventions that can be minimized to physiological ranges with proper selection of the needle length, needle position, and modification of pulse sequence parameters.

Materials and Methods: We simulated a clinical interventional MRI setting with 2 standard American Society for Testing and Materials F2182-11A phantoms and measured temperatures with fiber optic sensors. Temperature profiles were monitored for commercial 10, 15 and 20 cm MR-conditional cobalt-chromium needles in clinically relevant perpendicular, 45-degree oblique, and parallel orientations relative to the static magnetic field (B_0) and center, right off-center, and left off-center needle tip locations in the *z* = 0 plane. Clinically available interventional MRI pulse sequences including turbo spin echo (TSE), fast TSE, slice encoding for metal artifact correction, compressed sensing slice encoding for metal artifact correction, half-Fourier acquisition single-shot TSE (HASTE), HASTE inversion recovery, fluoroscopic steady-state gradient echo (3.0 T only), fast low-angle shot gradient echo, and volumetric interpolated breath-hold examination gradient echo pulse sequences were tested at 1.5 and 3.0 T field strengths. Acquired temperature data were analyzed using Friedman and Wilcoxon signed-rank tests with Bonferroni correction.

Results: After 5-minute of continuous MRI, less than 2.5°C heating occurred when needles were oriented perpendicular and 45-degree oblique to B_0, regardless of field strengths. Higher temperature rises capable of causing permanent tissue damage were observed when needles were oriented in parallel to B_0 (1.5 T: 22°C with 20 cm needles, 3.0 T: 8°C with 10 and 15 cm needles) using higher radiofrequency energy pulse sequences, such as TSE and HASTE. Left off-center location, parallel orientation, and needle lengths close to half of the radiofrequency pulse wavelength were positively associated with higher temperature rises.

Conclusions: Under the herein used experimental conditions, clinically used MR-conditional needles can heat to supraphysiologic temperatures during prolonged MRI at 1.5 and 3.0 T field strengths; however, the temperature rise can be balanced to physiological ranges with proper selection of needle length, needle orientation, and pulse sequence parameters. Caution must be exercised when using different MRI systems, as results may not directly translate.

Received for publication November 14, 2019; and accepted for publication, after revision, December 12, 2019.

From the *Department of Radiology, New York University School of Medicine, New York, NY; and †Russell H. Morgan Department of Radiology and Radiological Science, Johns Hopkins University School of Medicine, Baltimore, MD.

Conflicts of interest and sources of funding: This study received Radiologic Society of North America Fellow Research Grant (I.K.) and Society of Interventional Radiology Dr. and Mrs. W.C. Culp Student Research Grant (L.W.B.). Dr Weiss receives grant support from Siemens Healthcare, BTG/Boston Scientific, and Medtronic. Jan Fritz received institutional research support from Siemens Healthcare USA, DePuy, Zimmer, Microsoft, and BTG International; is a scientific advisor of Siemens Healthcare USA, GE Healthcare Technologies, and BTG International; received speaker's honorarium from Siemens Healthcare USA; and has shared patents with Siemens Healthcare and Johns Hopkins University.

Correspondence to: Jan Fritz, MD, PD, DABR, RMSK, New York University Grossman School of Medicine, Department of Radiology, 660 1st Ave, 3rd Floor Rm #313, New York, NY 10016. E-mail: jan.fritz@nyulangone.org.

ISSN: 0020-9996/20/5506–0396
DOI: 10.1097/RLI.0000000000000649

Key Words: interventional MRI, biopsy needle, radiofrequency heating, 1.5 T, 3 T

(*Invest Radiol* 2020;55: 396–404)

Magnetic resonance imaging (MRI)–guided interventions have grown in popularity over the past 2 decades with compelling uses that drove new developments and replacement of other modalities for select biopsies, nerve blocks, thermal ablations, drainages, and vascular interventions.[1–12] However, metallic interventional instruments pose safety risks that need to be addressed before each application. One major concern is radiofrequency (RF)-induced instrument heating, in which the electric field of the transmit coil couples with elongated conductive devices and amplifies the local specific absorption rate (SAR) of the RF energy deposition.[13] Such increased energy deposition may produce excessive heating, which can induce tissue damage as reported in some cases.[14,15]

Various factors, such as device configuration, coating, positioning within the scanner and patient, and device length are critical factors for RF-induced heating. Coupling (resonant) effects between a conductive device and RF pulse occur when the device dimension is between the half- and full-wavelength of the RF pulse within the body, which can lead to excessive heating. The half-wavelength of the RF field inside a patient is approximately 25 cm at 1.5 T systems and 12 cm at 3.0 T systems. Notably, excessive heating may occur with devices that do not have the exact resonant length, and to add to the complexity, the length of maximum heating has been shown to shift toward the quarter-wavelength in some cases.[16–19] Therefore, it is imperative to understand heating potentials of different device categories, for example, needles, with respect to their use in a clinical interventional MRI setting.

Previous studies investigating RF-induced heating focused on 1.5 T field strength and describe widely varying results depending on the utilized instrument, exposure protocol, and experimental setup.[13,18–27] However, the clinical use of 3.0 T systems in MRI-guided procedures continues to grow for injection and biopsy procedures using MR-conditional cobalt-chromium needles,[28–30] which merit further thermal safety evaluation. Moreover, recently developed metal artifact reduction MRI pulse sequences, such as slice encoding for metal artifact correction (SEMAC), improve visualization of needle position and trajectory compared with conventional pulse protocols and thus should similarly undergo thermal safety evaluation.[31–33]

Therefore, we designed this study to provide systemic and empiric data on the thermal safety profile of MRI-conditional needles at 1.5 and 3.0 T. Specifically, we tested the hypothesis that clinically used MR-conditional needles of varying lengths, orientations, locations, and pulse sequences can result in excessive heating during MRI-guided interventions that can be minimized to physiological ranges with proper selection of the needle length, needle position, and modification of pulse sequence parameters.

MATERIALS AND METHODS

Magnetic Resonance Imaging Equipment

We used clinical 1.5 T (Magnetom Aera; Siemens Healthineers, Erlangen, Germany) and 3.0 T (Magnetom Skyra; Siemens Healthineers) wide-bore MRI systems. Both systems are being used for MRI-guided

interventional procedures at our and other institutions worldwide with signal transmission through the built-in body coils and receive-only surface coils for signal collection.

Experimental Setup

Two rectangular human torso MRI phantoms were designed according to the American Society for Testing and Materials (ASTM) F2182-11A standard, which defines the guidelines to measure the RF heating induced by medical devices in standard phantoms filled with gelled saline mimicking the thermal and electrical properties of human muscle.[34] The phantoms were placed head-to-head on the MRI system's table to simulate the upper and lower parts of a 40-year-old human torso with a height of 180 cm and weight of 80 kg. The surface coils were positioned on top of needle-containing phantoms resembling our setup in patients (Fig. 1A).

Commercially available MR-conditional 20-gauge cobalt-chromium Chiba-type injection needles (Cook Medical, Bloomington, IN) with 10, 15, and 20 cm lengths were mounted on nonconducting plastic holders and immersed in the gel medium. Each needle was tested in 3 different orientations in the *y*-*z* plane (parallel, oblique, and perpendicular with 0-, 45-, and 90-degree angles relative to the static magnetic field [B_0], respectively; Fig. 1B). Irrespective of the needle orientation, the tip of the needle was always placed at the *x*-*y* plane (z = 0) of the magnet because this plane represents the practical case in the majority of interventional MRI procedures. To account for spatial variations of the RF power deposition in the *x*-*y* plane in the isocenter ($z = 0$) and to evaluate the extreme cases of heating for each needle length and orientation, needles were tested in 3 different locations along the *x*-axis in the isocenter ($z = 0$ plane). One needle was placed in the geometrical center of the *x*-axis, and 2 needles were placed in a right lateral and left lateral off-center locations at $x = \pm 13$ cm equidistantly to the center (Fig. 1D), as this represents the *x*-axis range of needle placements in the majority of our MRI-guided interventions. For perpendicular and oblique orientations, approximately 4.5 cm of the needle length was immersed in the gel, whereas for parallel cases the entire needle length was submerged.

Fiber optic sensors (Neoptix Inc, Québec City, Québec, Canada) with 0.1°C accuracy range and 1-Hz sampling rate were used to measure the temperature changes at the needle tips and shafts approximately 10 cm away from the needle tip. Sensor crystals were within 2 mm of the needle tip (Fig. 1C). To monitor the temperature changes of the gel medium for internal control, an additional sensor was placed at the bottom of the phantom far from the needles.

Interventional MRI Pulse Sequences

We used a variety of pulse sequences that are typically used for device visualization and monitoring during MRI-guided procedures including turbo spin echo with 20% phase-oversampling (TSE), TSE without phase-oversampling (TSE-FAST), SEMAC, compressed sensing SEMAC (CS-SEMAC),[35] half-Fourier acquisition single-shot TSE (HASTE), HASTE inversion recovery (HASTE-IR), fluoroscopic steady-state gradient echo pulse sequence (FLUORO, 3.0 T only), static fast low-angle shot (FLASH) gradient echo, and volumetric interpolated breath-hold examination (VIBE) gradient echo (Table 1). All sequences usually have clinical acquisition times between 1 and 60 seconds. However, to accentuate subtle temperature changes and emulate the effects of successive image acquisition during procedures, each sequence was acquired continuously for 5 minutes.

Statistical Analysis

All statistical analyses were performed using SPSS 22 (SPSS Inc, Chicago, IL). Ratios are reported as percentages with 95% confidence intervals (95% CIs). The normality of the data was tested with a Shapiro-Wilk test. Because the residuals failed to follow a normal distribution, the nonparametric Friedman test was implemented for multigroup comparisons. Degree of freedom, Friedman χ^2, and level of significance (*P* value) were presented for each case. This was followed by post hoc analysis using the Wilcoxon signed-rank test with Bonferroni correction to evaluate the difference in temperature rises among different

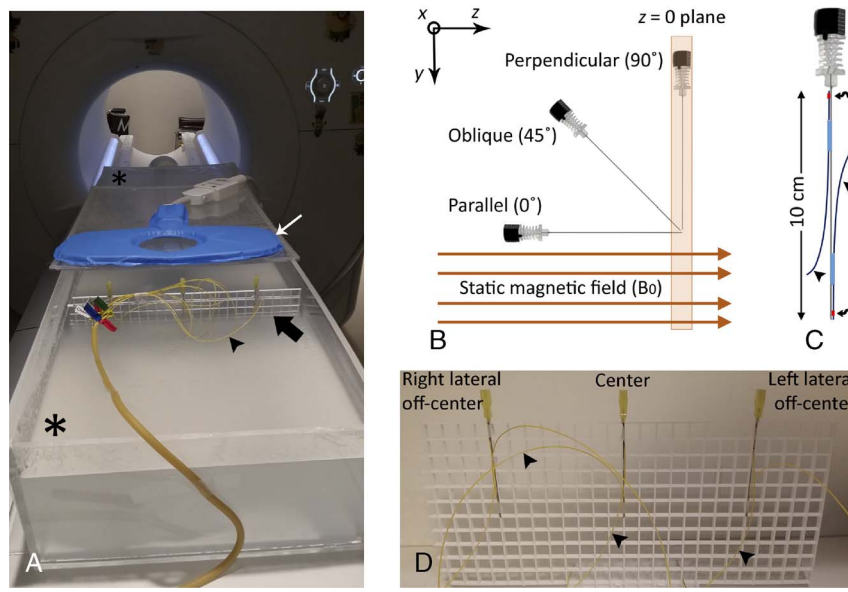

FIGURE 1. A, Experimental setup including 2 American Society for Testing and Materials (ASTM) gel phantoms (asterisks), receiver coil (thin white arrow), acrylic needle mount (thick black arrow), and temperature sensors (arrowhead). B, Tested needle orientations: parallel, oblique, and perpendicular with respective 0-, 45-, and 90-degree orientations relative to the static magnetic field B_0. C, Temperature probes (arrowheads) taped along the needle with the sensors (curved arrows) within 2 mm of the needle tip and 10 cm proximally along the shaft. D, Tested needle locations and accompanying temperature probes (arrowheads): *x*-axis center and equidistantly 13 cm off-center at each side.

needle locations, orientations, and lengths as well as across various pulse sequences. To identify the association between the needle temperature rises under each pulse sequence and the relevant whole-body SARs, linear regression and correlation coefficients (R) were used. A P value of less than 0.05 was considered statistically significant.

RESULTS

Temperature changes after 5 minutes of continuous MRI (ΔT_{5min}) were higher at the needle tip than at the shaft location in 99.5% of the cases at 1.5 T (95% CI, 87%–100%, $P < 0.0001$) and 97% of the cases at 3.0 T (95% CI, 85%–100%, $P < 0.01$), accounting for temperature sensor error margins of 0.1°C. Hence, from this point forward, we will present the data related to temperature changes at the needle tip.

Effect of Needle Location

At 1.5 T, ΔT_{5min} was significantly different at different needle locations along the x-axis at $z = 0$ ($\chi^2[2] = 66.637$, $P < 0.00001$). Post hoc analysis showed higher ΔT_{5min} for the left lateral off-center than the center location ($Z = -5.843$, $P < 0.00001$), left lateral off-center than right lateral off-center location ($Z = -5.919$, $P < 0.00001$), and center than right lateral off-center location ($Z = -3.377$, $P = 0.0007$). Overall, ΔT_{5min} was greatest at the left lateral off-center location, specifically 3.93 times higher than center and 5.81 times higher than right lateral off-center locations for 20 cm needles in parallel orientation (Fig. 2A).

At 3.0 T, ΔT_{5min} was significantly different at different needle locations in the x-axis at $z = 0$ ($\chi^2[2] = 48.076$, $P < 0.00001$). Post hoc analysis showed higher ΔT_{5min} for the left lateral off-center than center location ($Z = -6.382$, $P < 0.00001$), and left lateral off-center than right lateral off-center location ($Z = -5.533$, $P < 0.00001$). There was no significant difference between the center and right lateral off-center location ($Z = -0.744$, $P = 0.457$). Overall, ΔT_{5min} was greatest at the left lateral off-center location, specifically 1.47 times higher than center and 1.49 times higher than right lateral off-center locations, for 15 cm needles in parallel orientation (Fig. 2B).

Temperature Rises

Table 2 shows ΔT_{5min} of the needle tips for various needle lengths, orientations, and field strengths. Presented data are those of the left lateral off-center location, as this was the location with the highest degree of heating. For the perpendicular orientation, needle heating did not exceed 0.5°C irrespective of needle length, needle location (center vs off-center), and magnetic field strength. Greater temperature increases of up to 2.5°C occurred with the oblique needle orientations at 45° to B_0. Heating of up to 8°C (15 cm needle at 3.0 T) and 22°C (20 cm needle at 1.5 T) occurred at the tip of needles oriented parallel to B_0. Further data analysis showed that after 30 seconds of acquisition time with high SAR pulse sequences (eg, TSE or HASTE) and a 20 cm needle oriented parallel to the 1.5-T magnetic field can cause temperature rise greater than 10°C (see below).

Effects of Needle Length and Orientation

Because from a physics standpoint only the longitudinal needle component along the B_0 contributes to RF heating, we calculated the longitudinal component as the needle length times the cosine of the angle formed by the needle and B_0 (Fig. 3).

There were significant dependencies of ΔT_{5min} on needle orientation and length at both field strengths (1.5 T: $\chi^2[8] = 102.017$, $P < 0.00001$, 3.0 T: $\chi^2[8] = 172.295$, $P < 0.00001$). Post hoc analysis of pair-wise comparisons (Table 3) shows inverse associations between heating and the angle formed by the needle and B_0 magnetic field, meaning that there were higher temperature rises for orientations that were closer aligned in parallel with B_0. Needle length had no effect on the temperature rise when needles were oriented perpendicular to B_0, as no substantial heating occurred with this orientation. However, longer needles heated more when aligned in parallel with B_0. At 1.5 T, the maximum heating effects occurred with

TABLE 1. MRI Pulse Sequence Parameters

	Whole-Body SAR, W/kg (90/45/0 degrees)								
	10 cm	15 cm	20 cm	Flip Angle	Resolution	Bandwidth (Hz/Pixel)	Voxel Size (mm)	Echo Spacing (ms)	Turbo Factor
1.5 T									
TSE	1.62/1.56/1.59	1.62/1.59/1.60	1.58/1.58/1.58	150	350 × 263	482	0.9 × 0.9 × 2.5	7.24	25
TSE-FAST	1.62/1.56/1.59	1.62/1.59/1.60	1.62/1.58/1.61	150	350 × 263	482	0.9 × 0.9 × 2.5	7.24	25
SEMAC	0.19/0.21/0.22	0.19/0.21/0.22	0.18/0.21/0.18	130	350 × 263	413	0.8 × 0.8 × 2.5	8.12	23
CS-SEMAC	0.37/0.43/0.44	0.37/0.44/0.44	0.36/0.42/0.36	130	350 × 263	413	0.8 × 0.8 × 2.5	8.12	23
HASTE	1.60/1.55/1.59	1.59/1.58/1.60	1.60/1.57/1.60	180	350 × 263	482	0.9 × 0.9 × 2.5	5.38	288
HASTE-IR	1.41/1.56/1.58	1.42/1.59/1.59	1.37/1.57/1.38	150	350 × 263	300	1.1 × 1.1 × 4.0	5.92	240
FLASH	0.06/0.06/0.07	0.06/0.06/0.07	0.05/0.06/0.05	20	350 × 350	410	0.9 × 0.9 × 3.0	NA	NA
VIBE	0.21/0.24/0.25	0.21/0.25/0.25	0.20/0.24/0.20	9.5	350 × 350	410	0.9 × 0.9 × 2.5	NA	NA
3.0 T									
TSE	1.23/1.23/1.29	1.11/1.17/1.30	1.31/1.31/1.30	150	512 × 384	488	0.7 × 0.7 × 2.5	9.44	25
TSE-FAST	1.19/1.19/1.23	1.08/1.13/1.27	1.27/1.27/1.26	150	512 × 384	488	0.7 × 0.7 × 2.5	9.44	25
SEMAC	0.17/0.17/0.18	0.16/0.16/0.18	0.18/0.18/0.18	130	512 × 384	407	0.7 × 0.7 × 2.5	8.58	23
CS-SEMAC	0.30/0.30/0.32	0.27/0.29/0.32	0.32/0.32/0.32	130	512 × 384	407	0.7 × 0.7 × 2.5	8.58	23
HASTE	1.09/1.09/1.15	0.99/1.04/1.16	1.16/1.16/1.16	180	512 × 512	488	0.7 × 0.7 × 2.5	6.5	384
HASTE-IR	1.26/1.26/1.32	1.13/1.19/1.33	1.34/1.34/1.33	180	384 × 384	303	0.9 × 0.9 × 4.0	6.92	288
FLUORO	0.21/0.21/0.22	0.19/0.20/0.22	0.22/0.22/0.22	30	256 × 256	558	1.2 × 1.2 × 3.0	4.7	NA
FLASH	0.09/0.09/0.09	0.08/0.08/0.09	0.09/0.09/0.09	20	512 × 460	410	0.7 × 0.7 × 3.0	NA	NA
VIBE	0.29/0.29/0.31	0.26/0.28/0.31	0.31/0.31/0.31	9.5	512 × 512	410	0.7 × 0.7 × 2.5	NA	NA

MRI indicates magnetic resonance imaging; SAR, specific absorption rate; TSE, turbo spin echo with 20% phase-oversampling; TSE-FAST, TSE without phase-oversampling; SEMAC, slice encoding for metal artifact correction; CS-SEMAC, compressed sensing SEMAC; HASTE, half-Fourier acquisition single-shot TSE; HASTE-IR, HASTE inversion recovery; FLUORO, fluoroscopic steady-state gradient echo; FLASH, static fast low-angle shot gradient echo; VIBE, volumetric interpolated breath-hold examination gradient echo.

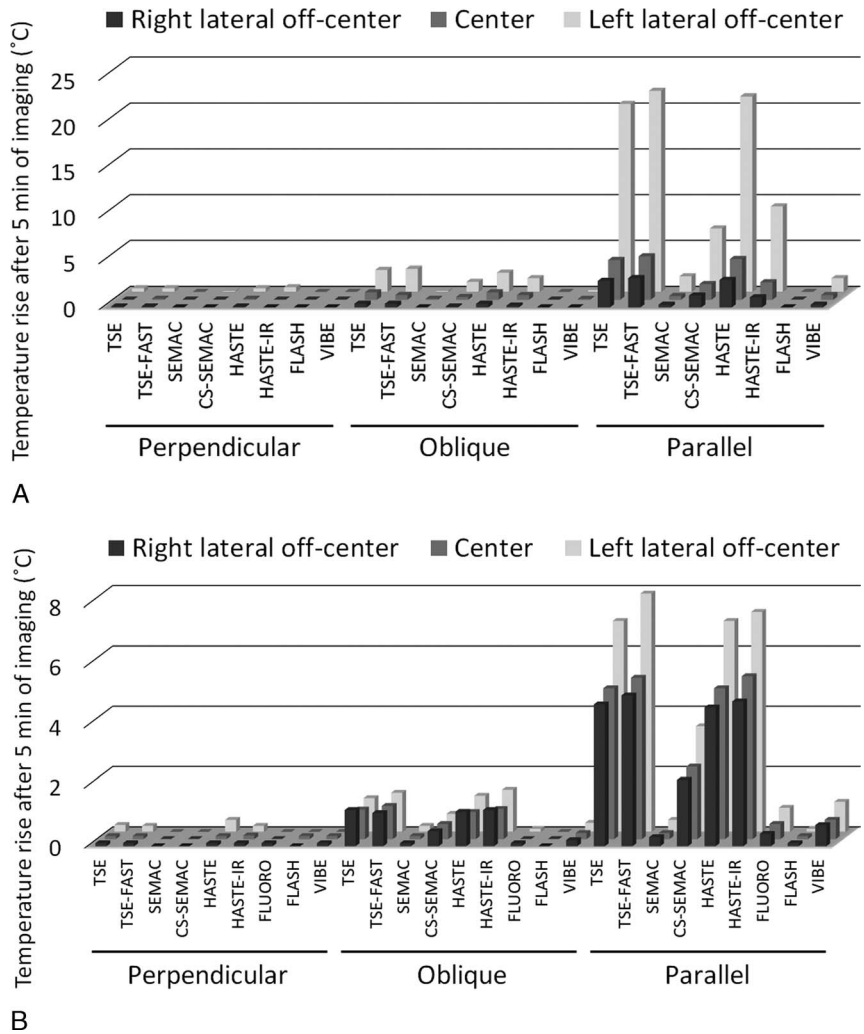

FIGURE 2. Temperature rises at the needle tip after 5 minutes of continuous MRI using different pulse sequences as a function of needle location for 20 cm needles at 1.5 T (A) and 15 cm needles at 3.0 T (B). For visualization purposes, these particular needle lengths were chosen as they were associated with greater degrees of heating.

the 20 cm needle in parallel orientation, whereas 10 and 15 cm parallel needles produced the maximum heating at 3.0 T.

Effects of MRI Pulse Sequences

Needle heating significantly differed at 1.5 T ($\chi^2[7] = 140.970$, $P < 0.00001$) and 3.0 T ($\chi^2[8] = 170.983$, $P < 0.00001$) depending on the applied MRI pulse sequence. At 1.5 T, the TSE, TSE-FAST, and HASTE pulse sequences averaged across all locations and orientation resulted in higher heating compared with other pulse sequences (pair-wise, $P < 0.0001$; Fig. 4A). At 3.0 T, the TSE, TSE-FAST, HASTE, and HASTE-IR pulse sequences resulted in higher heating than the other pulse sequences (pair-wise $P < 0.0001$; Fig. 4B).

The 4 pulse sequences (TSE, TSE-FAST, HASTE, HASTE-IR) resulting in the highest temperature rise also had the highest whole-body SAR values with high statistical correlations between temperature rise and whole-body SAR (Fig. 5).

DISCUSSION

With the purpose to emulate clinical practice settings of interventional MRI, we utilized 2 commonly employed magnetic field strengths (1.5 and 3.0 T), a variety of clinically available traditional and novel interventional MRI pulse sequences, and cobalt-chromium needles of different lengths at different locations and orientations within the bore of the MRI systems, in order to explore the potential for needle heating during MRI-guided interventional procedures. We chose cobalt-chromium needles for this study as they constitute the majority of commercially available MR-conditional needles and what we use clinically for MRI-guided interventional procedures. For 1.5 and 3.0 T, all pulse sequences, 10, 15, and 20 cm needle lengths, and needle orientations between 45° to 90° relative to B_0, heating of the needle tip was minimal ($\Delta T_{5min} < 2.5$°C) and stayed within the physiological range during 5 minutes of continuous MRI. However, with needles oriented in parallel relative to B_0, supraphysiological and potentially harmful heating occurred, which was maximized for 20 cm long needles (ΔT_{5min}=22°C) at 1.5 T and 10 and 15 cm long needles (ΔT_{5min}=8°C) at 3.0 T. We designed our study to elucidate this practically important question and provide practical safety parameters that can be applied by technologists and interventionalists during interventional MRI procedures. Specifically, our results provide guidance for appropriate selection of needle lengths and orientations as well as type and timing of the MR pulse sequence to ensure patient safety.

Previous data suggest that MR-compatible wires and catheters are safe at 1.5 T when positioned properly and at wire and catheter lengths well beyond or less than the critical length[19,20] but otherwise

TABLE 2. Temperature Rise of the Tip of the Needle in the Left Lateral Off-Center Location After 5 Minutes of Continuous Imaging (ΔT_{5min}) for Different Needle Lengths and Orientations

		ΔT_{5min} (°C) of Left Needle Tip/ΔT_{5min} (°C) of Gel Medium Serving as Control								
Needle	**Orientation**	**TSE**	**TSE-FAST**	**SEMAC**	**CS-SEMAC**	**HASTE**	**HASTE-IR**	**FLUORO**	**FLASH**	**VIBE**
1.5 T										
10 cm	Perpendicular	0.3/0.1	0.3/0.1	0.0/0.0	0.0/0.0	0.3/0.2	0.2/0.1	—	0.0/0.0	0.0/0.0
	Oblique	1.6/0.0	1.8/0.1	0.0/0.0	0.4/0.0	1.4/0.1	0.5/0.1	—	0.0/0.0	0.1/0.0
	Parallel	6.9/0.1	8.5/0.0	0.0/0.1	3.1/0.1	5.9/0.3	2.9/0.0	—	0.0/0.0	0.6/0.1
15 cm	Perpendicular	0.1/0.0	0.1/0.0	0.0/0.0	0.0/0.1	0.2/0.0	0.2/0.1	—	0.0/0.0	0.0/0.0
	Oblique	1.2/0.1	2.1/0.1	0.0/0.0	0.3/0.0	1.2/0.1	0.5/0.0	—	0.0/0.0	0.0/0.0
	Parallel	12.1/0.1	16.4/0.0	0.0/0.1	5.9/0.0	9.7/0.1	3.4/0.0	—	0.0/0.0	1.0/0.1
20 cm	Perpendicular	0.4/0.1	0.4/0.1	0.0/0.0	0.1/0.1	0.4/0.0	0.5/0.1	—	0.0/0.0	0.0/0.1
	Oblique	2.4/0.1	2.5/0.1	0.1/0.1	1.1/0.0	2.1/0.0	1.5/0.1	—	0.0/0.0	0.2/0.0
	Parallel	20.5/0.0	21.9/0.1	1.7/0.0	6.9/0.0	21.3/0.0	9.3/0.0	—	0.0/0.0	1.5/0.0
3.0 T										
10 cm	Perpendicular	0.2/0.3	0.2/0.3	0.0/0.0	0.1/0.1	0.2/0.2	0.1/0.3	0.0/0.0	0.0/0.0	0.0/0.0
	Oblique	0.9/0.3	1.4/0.3	0.0/0.0	0.5/0.1	0.8/0.2	0.7/0.2	0.0/0.0	0.0/0.0	0.2/0.0
	Parallel	7.1/0.1	7.3/0.1	0.7/0.1	3.3/0.1	6.0/0.1	7.7/0.0	0.4/0.0	0.0/0.0	1.1/0.0
15 cm	Perpendicular	0.2/0.2	0.2/0.2	0.0/0.0	0.0/0.2	0.4/0.3	0.2/0.3	0.0/0.0	0.0/0.0	0.0/0.0
	Oblique	1.1/0.6	1.3/0.6	0.2/0.0	0.6/0.2	1.2/0.3	1.4/0.3	0.1/0.0	0.0/0.0	0.3/0.0
	Parallel	7.0/0.1	7.9/0.1	0.4/0.1	3.5/0.0	7.0/0.1	7.3/0.1	0.8/0.0	0.1/0.0	1.0/0.1
20 cm	Perpendicular	0.3/0.3	0.3/0.3	0.1/0.0	0.1/0.1	0.1/0.3	0.2/0.3	0.0/0.1	0.0/0.0	0.0/0.0
	Oblique	1.7/0.3	2.0/0.4	0.0/0.0	0.6/0.1	1.6/0.5	1.7/0.3	0.2/0.0	0.0/0.0	0.2/0.0
	Parallel	4.0/0.1	3.9/0.1	0.4/0.1	1.9/0.0	3.9/0.1	4.2/0.1	0.4/0.0	0.0/0.0	0.7/0.0

TSE indicates turbo spin echo with 20% phase-oversampling; TSE-FAST, TSE without phase-oversampling; SEMAC, slice encoding for metal artifact correction; CS-SEMAC, compressed sensing SEMAC; HASTE, half-Fourier acquisition single-shot TSE; HASTE-IR, HASTE inversion recovery; FLUORO, fluoroscopic steady-state gradient echo; FLASH, static fast low-angle shot; VIBE, volumetric interpolated breath-hold examination.

can heat in excess of 30°C.[20] Although the principles governing device heating during interventional MRI were developed decades ago,[36,37] important gaps in our knowledge exist about how specific device categories heat during MRI, especially with respect to needle heating, more recently developed sequences designed to optimize needle visualization, and interventional MRI at 3.0 T.

Data about instrument heating at 3.0 T are sparse. Theoretical 3.0 T predictions[38] align with our measured results, which showed a maximal heating of 8°C with needle lengths of 10 or 15 cm lengths, both of which are close to the critical length of 12 cm. Accordingly, selection of needle lengths shorter or longer than the critical length seems a suitable approach to minimize heating. Our findings at 1.5 T are in agreement

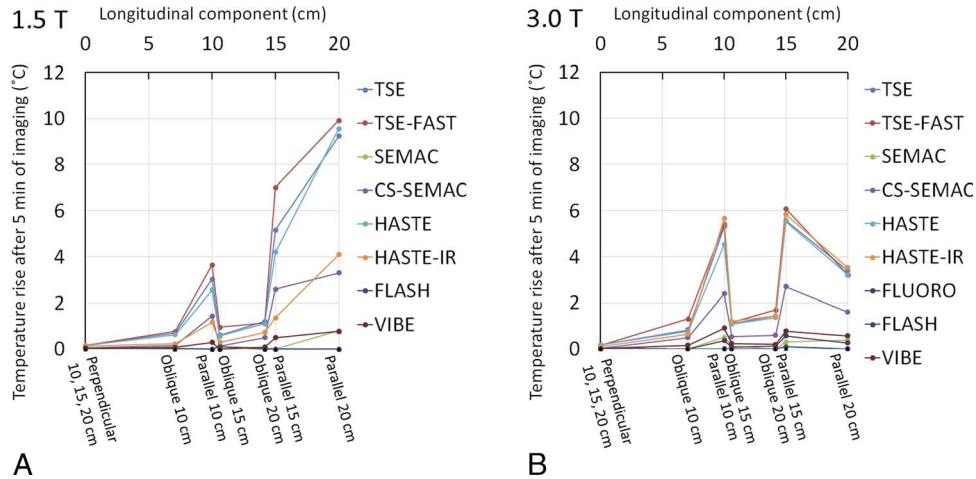

FIGURE 3. Mean temperature rises after 5 minutes of continuous MRI as a function of the longitudinal component of the needle length and pulse sequence for different needle lengths and orientations at 1.5 T (A) and 3.0 T (B) magnetic fields. The longitudinal component was calculated for each needle using the needle length and angle relative to B_0. As oblique needles were oriented at 45-degree relative to B_0, the effective longitudinal component of the needle was the needle's length divided by $\sqrt{2}$. TSE indicates turbo spin echo with 20% phase-oversampling; TSE-FAST, TSE without phase-oversampling; SEMAC, slice encoding for metal artifact correction; CS-SEMAC, compressed sensing SEMAC; HASTE, half-Fourier acquisition single-shot TSE; HASTE-IR, HASTE inversion recovery; FLUORO, fluoroscopic steady-state gradient echo; FLASH, static fast low-angle shot gradient echo; VIBE, volumetric interpolated breath-hold examination gradient echo.

TABLE 3. Bonferroni Corrected *P* Values for Pair-Wise Needle Length/Orientation Comparisons

	Perpendicular 10 cm	Oblique 10 cm	Parallel 10 cm	Perpendicular 15 cm	Oblique 15 cm	Parallel 15 cm	Perpendicular 20 cm	Oblique 20 cm	Parallel 20 cm
Perpendicular 10 cm		>0.05	0.006	>0.05	0.013	0.006	>0.05	0.008	0.002
Oblique 10 cm	0.004		0.008	>0.05	>0.05	0.006	0.014	0.011	0.002
Parallel 10 cm	0.000	0.001		0.018	0.020	0.013	0.007	0.021	0.002
Perpendicular 15 cm	>0.05	0.008	0.000		>0.05	0.015	>0.05	>0.05	0.001
Oblique 15 cm	0.001	>0.05	0.001	0.001		0.013	0.004	>0.05	0.001
Parallel 15 cm	0.000	0.000	>0.05	0.000	0.000		0.007	0.012	0.003
Perpendicular 20 cm	>0.05	0.005	0.001	>0.05	0.001	0.000		0.005	0.002
Oblique 20 cm	0.002	0.003	0.001	0.003	>0.05	0.000	0.002		0.002
Parallel 20 cm	0.000	0.001	0.002	0.001	0.001	0.001	0.001	0.001	

The clear top right part portion of the table shows the results of 1.5 T data while the shaded bottom left corner shows those of 3.0 T.

with previous studies, showing a maximal heating of 22°C after 5 minutes of MRI with use of 20 cm long MR-compatible needle, which is close to the critical length of 25 cm.[16–19]

With respect to needle position at the $z = 0$ axial plane, we found consistently higher heating at the left lateral off-center location for both 1.5 and 3.0 T. As shown in a recent study,[39] the rectangular shape of the ASTM phantom can result in an ellipsoidal distribution of the longitudinal electric field and asymmetrical heating in lateral locations. This asymmetric effect was more pronounced at our 1.5 T than 3.0 T experiments, which may be related to the hard-coded RF pulse polarization. The 1.5 T MRI systems used circularly polarized RF pulse polarization, whereas the 3.0 T MRI systems used elliptical RF pulse polarization capable of producing more uniform B_1 distribution in rectangular geometries.

In our experiments, the effect of needle length was less pronounced in oblique orientations. In addition, needles oriented in parallel to B_0 caused higher temperature rises when compared with the obliquely oriented needles of comparable longitudinal component (drop in temperature curves of Fig. 3), which may be because the oblique needles had shorter portions immersed in the gel compared with fully submerged parallel needles. In agreement with a previous study,[40] this finding suggests that in addition to the needle length, the portion of the needle that is within the patient's body influences the degree of heating.

As needle orientation relative to B_0 has a major influence on needle heating, the architecture of the MRI systems used for interventional MRI deserves special consideration. Many interventional MRI procedures of the musculoskeletal system and abdominal organs are best performed with needle paths in the axial plane,[28,41] which poses low risk for thermal injury. However, applications using a longitudinal needle path with the needle oriented in parallel to B_0, which may occur more often with brain, breast, and prostate interventions, pose an increased risk for thermal injury. In such cases, alternative needle paths, MRI systems with vertically oriented B_0, and optimized MRI pulse sequences can minimize this risk.[42,43]

Although there is no general correlation between metal-induced heating and whole-body SAR due to varying positioning and configuration of metallic hardware as well as different SAR estimation methods across various vendors,[44] our controlled experiments with needles kept in similar location found a positive linear correlation between estimated whole-body SAR values and needle heating. As such, modifications to MRI pulse sequences aiming to decrease SAR will decrease the risk of

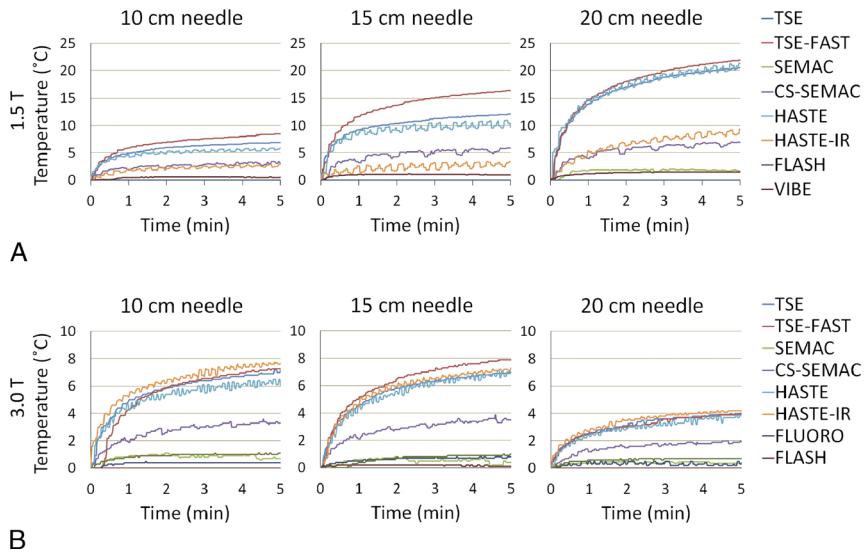

FIGURE 4. Temperature rises of the left-sided needles in parallel orientation for various pulse sequences at 1.5 T (top) and 3.0 T (bottom) magnetic fields. TSE indicates turbo spin echo with 20% phase-oversampling; TSE-FAST, TSE without phase-oversampling; SEMAC, slice encoding for metal artifact correction; CS-SEMAC, compressed sensing SEMAC; HASTE, half-Fourier acquisition single-shot TSE; HASTE-IR, HASTE inversion recovery; FLUORO, fluoroscopic steady-state gradient echo; FLASH, static fast low-angle shot gradient echo; VIBE, volumetric interpolated breath-hold examination gradient echo.

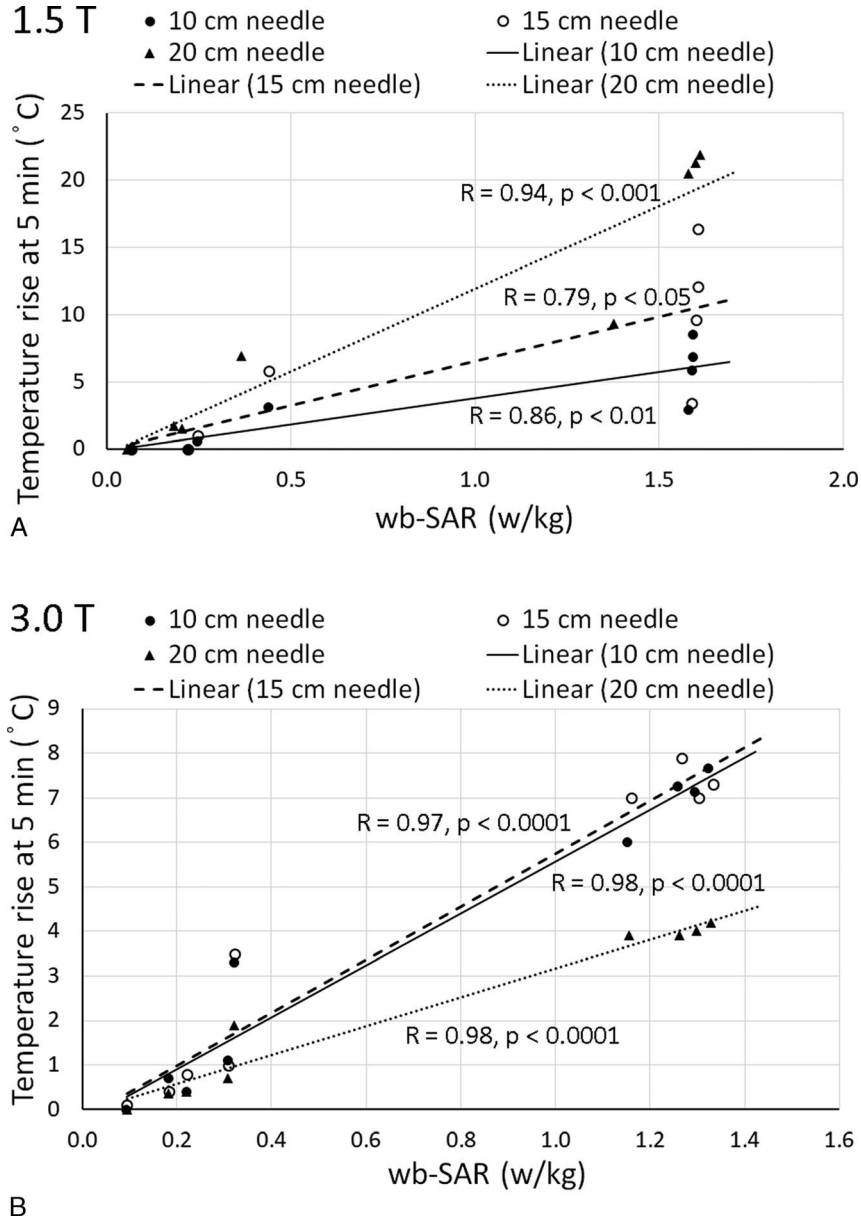

FIGURE 5. Dependency of maximum needle heating on the MRI system-estimated whole-body specific absorption rate (SAR) for various pulse sequences at 1.5 T (A) and 3.0 T (B). There are direct correlations between temperature rise and whole-body SAR. *R* indicates correlation coefficient; linear, linear trend.

metal-related heating. To achieve this, 3 strategies can be applied during interventional MRI procedures: (1) decrease the number of RF pulses by using gradient echo-based instead of spin echo-based pulse sequences, reducing the number of slices, reducing the number of phase encoding steps through decreased field of view and matrix size, or using partial Fourier imaging, and occasionally employing parallel imaging depending how other parameters are adjusted; (2) decrease the energy of each pulse by decreasing the flip angle, using low SAR RF pulse profiles, and using low transmission bandwidth; and (3) prolonging the scan duration by introducing gaps between successive pulse sequences and increasing the repetition time.

In agreement with these strategies, we measured lower temperature rises with the gradient echo-based sequences used for this study. Similarly, accelerated compressed sensing-based sampling was associated with higher temperature rises as it decreases the repetition time. A practically important consideration is that some modifications, including using gradient echo sequences and low transmission bandwidth, result in increased metal-related susceptibility artifacts and may have limited applicability depending on the procedure.

Our study has limitations. First, we included 2 wide-bore MRI systems and a variety of commonly used pulse sequences that we use for interventional MRI. Although the physical principals underlying the needle heating likely apply to other MRI systems and pulse sequences, our data may not be extended easily to other systems and pulse sequence designs, even from the same manufacturer, warranting individual testing in order to obtain specific empiric evidence for safety prognostications. In particular, our finding of greater heating of left-sided off-center needles could be different in other MRI systems with a different body coil design. Other pulse sequences, such as diffusion-weighted imaging, which can help to target suspicious areas within a lesion,[45,46] real-time pulse sequences with nonconventional acquisitions,[47] and faster techniques such as simultaneous multislice imaging,[48,49] may pose a

risk of thermal injury and should be tested as well. Second, we used clinically available needle length to closely mirror clinical practice. Despite using the ASTM F2182-11A standard, the purpose of the current study was not to determine the critical length of the needle or to safety label the needles through exploration of the worst cases of heating at extreme locations and high SAR values. In accordance with physics principles, heating is expected to be higher with critical lengths and high SAR values. Third, although we used a standard phantom to characterize the thermogenic profile of a variety of needles, needle locations, needle orientations, and pulse sequences, we did not confirm the temperature rise and occurrence of actual thermal injuries using animal models or human subjects. In a human or animal model, the heating we observed may be tempered by the dispersive effects of systemic circulation, which may result in overestimation of heating effects in our ATSM phantom-based setup. However, this setting would constitute an additional safety margin for patients, which can further minimize thermal injury risk and should not give grounds to obviate best practice and risk minimizing strategies when performing interventional MRI procedures. Although studies using clinically realistic in vivo models or even patients will be required to narrow approximation margins to the human body and gauge effects of heat dispersion via systemic circulation, they are practically difficult to obtain. Finally, our study was limited to one manufacturer's needles, and also did not consider other devices such as bone biopsy drills, ablation probes, and other devices that are frequently used during interventional MRI.

In conclusion, under the herein used experimental conditions, MR-conditional needles between perpendicular to 45-degree oblique orientation relative to the B_0 pose low risk of supraphysiological heating even after 5 minutes of continuous 1.5 and 3.0 T MRI with maximal heating of up to 2.5°C. However, if needles are placed parallel to B_0, potentially dangerous heating may occur, with maximal increases of approximately 22°C at 1.5 T and 8°C at 3.0 T. Practice strategies for interventionalist to reduce the risk of supraphysiological heating during MRI-guided procedures with needle orientation close to or parallel to B_0 include the use of needles that are longer or shorter than the critical length of 25 cm at 1.5 T and 12 cm at 3.0 T, and optimizing pulse sequence parameters to minimize the energy deposition, especially with pulse sequences with high SAR values such as TSE and HASTE. Caution must be exercised when using different MRI systems, as results may not directly translate.

REFERENCES

1. Weiss CR, Nour SG, Lewin JS. MR-guided biopsy: a review of current techniques and applications. *J Magn Reson Imaging*. 2008;27:311–325.
2. Fritz J, Dellon AL, Williams EH, et al. 3-tesla high-field magnetic resonance neurography for guiding nerve blocks and its role in pain management. *Magn Reson Imaging Clin N Am*. 2015;23:533–545.
3. Li C, Lü Y, Liu M, et al. Magnetic resonance imaging-guided biopsy of musculoskeletal lesions using open low-field systems. *Top Magn Reson Imaging*. 2011;22:135–141.
4. Kariniemi J, Blanco Sequeiros R, Ojala R, et al. MRI-guided abdominal biopsy in a 0.23-T open-configuration MRI system. *Eur Radiol*. 2005;15:1256–1262.
5. Schrading S, Strobel K, Keulers A, et al. Safety and efficacy of magnetic resonance-guided vacuum-assisted large-volume breast biopsy (MR-guided VALB). *Invest Radiol*. 2017;52:186–193.
6. Streitparth F, De Bucourt M, Hartwig T, et al. Real-time MR-guided lumbosacral periradicular injection therapy using an open 1.0-T MRI system: an outcome study. *Invest Radiol*. 2013;48:471–476.
7. Sequeiros RB, Sinikumpu JJ, Ojala R, et al. Pediatric musculoskeletal interventional MRI. *Top Magn Reson Imaging*. 2018;27:39–44.
8. Fritz J, U-Thainual P, Ungi T, et al. Augmented reality visualization using image overlay technology for MR-guided interventions: cadaveric bone biopsy at 1.5 T. *Invest Radiol*. 2013;48:464–470.
9. Ahrar K, Ahrar JU, Javadi S, et al. Real-time magnetic resonance imaging-guided cryoablation of small renal tumors at 1.5 T. *Invest Radiol*. 2013;48:437–444.
10. Carrino JA, Khurana B, Ready JE, et al. Magnetic resonance imaging-guided percutaneous biopsy of musculoskeletal lesions. *J Bone Joint Surg Am*. 2007;89:2179–2187.
11. Lu Y, Fritz J, Li C, et al. Magnetic resonance imaging-guided percutaneous biopsy of mediastinal masses: diagnostic performance and safety. *Invest Radiol*. 2013;48:452–457.
12. Krug KB, Ulhaas A, Hellmich M, et al. Impact of clinical and lesion characteristics on the results of MR-guided wire localizations of the breast using an open 1.0-T MRI system. *Invest Radiol*. 2013;48:445–451.
13. Nitz WR, Oppelt A, Renz W, et al. On the heating of linear conductive structures as guide wires and catheters in interventional MRI. *J Magn Reson Imaging*. 2001;13:105–114.
14. Spiegel J, Fuss G, Backens M, et al. Transient dystonia following magnetic resonance imaging in a patient with deep brain stimulation electrodes for the treatment of Parkinson disease. Case report. *J Neurosurg*. 2003;99:772–774.
15. Henderson JM, Tkach J, Phillips M, et al. Permanent neurological deficit related to magnetic resonance imaging in a patient with implanted deep brain stimulation electrodes for Parkinson's disease: case report. *Neurosurgery*. 2005;57:E1063; discussion E.
16. Kainz W. MR heating tests of MR critical implants. *J Magn Reson Imaging*. 2007;26:450–451.
17. Shellock FG. Comments on MR heating tests of critical implants. *J Magn Reson Imaging*. 2007;26:1182–1185.
18. Bassen H, Kainz W, Mendoza G, et al. MRI-induced heating of selected thin wire metallic implants—laboratory and computational studies—findings and new questions raised. *Minim Invasive Ther Allied Technol*. 2006;15:76–84.
19. Yeung CJ, Karmarkar P, McVeigh ER. Minimizing RF heating of conducting wires in MRI. *Magn Reson Med*. 2007;58:1028–1034.
20. Nyenhuis JA, Park S-M, Kamondetdacha R, et al. MRI and implanted medical devices: basic interactions with an emphasis on heating. *IEEE Trans Device Mater Reliab*. 2005;5:467–480.
21. Mattei E, Triventi M, Calcagnini G, et al. Complexity of MRI induced heating on metallic leads: experimental measurements of 374 configurations. *Biomed Eng Online*. 2008;7:11.
22. Nyenhuis JA. Interactions of medical implants with the magnetic fields in MRI. In: *Proceedings of the 25th Annual International Conference of the IEEE Engineering in Medicine and Biology Society (IEEE Cat. No.03CH37439), 17–21 Sept* vol. 4. 2003:3767–3770.
23. Liu CY, Farahani K, Lu DS, et al. Safety of MRI-guided endovascular guidewire applications. *J Magn Reson Imaging*. 2000;12:75–78.
24. Konings MK, Bartels LW, Smits HF, et al. Heating around intravascular guidewires by resonating RF waves. *J Magn Reson Imaging*. 2000;12:79–85.
25. Owens S, Erturk MA, Ouanes J-PP, et al. Evaluation of epidural and peripheral nerve catheter heating during magnetic resonance imaging. *Reg Anesth Pain Med*. 2014;39:534–539.
26. Mei L, Long X, Diao Y, et al. MRI evaluation of metal acupuncture needles. *Acupunct Med*. 2013;31:404–408.
27. Darcey TM, Kobylarz EJ, Pearl MA, et al. Safe use of subdermal needles for intraoperative monitoring with MRI. *Neurosurg Focus*. 2016;40:E19.
28. Fritz J, Dellon AL, Williams EH, et al. Diagnostic accuracy of selective 3-T MR neurography–guided retroperitoneal genitofemoral nerve blocks for the diagnosis of genitofemoral neuralgia. *Radiology*. 2017;285:176–185.
29. Tilak G, Tuncali K, Song SE, et al. 3T MR-guided in-bore transperineal prostate biopsy: a comparison of robotic and manual needle-guidance templates. *J Magn Reson Imaging*. 2015;42:63–71.
30. Penzkofer T, Tuncali K, Fedorov A, et al. Transperineal in-bore 3-T MR imaging-guided prostate biopsy: a prospective clinical observational study. *Radiology*. 2015;274:170–180.
31. Sonnow L, Gilson WD, Raithel E, et al. Instrument visualization using conventional and compressed sensing SEMAC for interventional MRI at 3T. *J Magn Reson Imaging*. 2018;47:1306–1315.
32. Lu W, Pauly KB, Gold GE, et al. SEMAC: slice encoding for metal artifact correction in MRI. *Magn Reson Med*. 2009;62:66–76.
33. Fritz J, Fritz B, Thawait GK, et al. Advanced metal artifact reduction MRI of metal-on-metal hip resurfacing arthroplasty implants: compressed sensing acceleration enables the time-neutral use of SEMAC. *Skeletal Radiol*. 2016;45:1345–1356.
34. American Society for Testing and Materials International. *Standard Test Method for Measurement of Radiofrequency Induced Heating on or Near Passive Implants During Magnetic Resonance Imaging: ASTM Standard F2182-11a, 2002*. West Conshohocken, PA: ASTM International; 2011.
35. Fritz J, Ahlawat S, Demehri S, et al. Compressed sensing SEMAC: 8-fold accelerated high resolution metal artifact reduction MRI of cobalt-chromium knee arthroplasty implants. *Invest Radiol*. 2016;51:666–676.

36. Atalar E. Radiofrequency safety for interventional MRI procedures. *Acad Radiol*. 2005;12:1149–1157.
37. Shellock FG. Radiofrequency energy-induced heating during MR procedures: a review. *J Magn Reson Imaging*. 2000;12:30–36.
38. Pictet J, Meuli R, Wicky S, et al. Radiofrequency heating effects around resonant lengths of wire in MRI. *Phys Med Biol*. 2002;47:2973–2985.
39. Bhusal B, Baig T, Bhattacharyya P, et al. *RF Heating Asymmetry in the Implants Placed at Opposite Lateral Halves of the ASTM Phantom. 27th Annual Meeting of the International Society for Magnetic Resonance in Medicine*. Montreal, Québec, Canada: International Society for Magnetic Resonance in Medicine; 2019.
40. Bhusal B, Bhattacharyya P, Baig T, et al. Measurements and simulation of RF heating of implanted stereo-electroencephalography electrodes during MR scans. *Magn Reson Med*. 2018;80:1676–1685.
41. O'Mara DM, DiCamillo PA, Gilson WD, et al. MR-guided percutaneous sclerotherapy of low-flow vascular malformations: clinical experience using a 1.5 tesla MR system. *J Magn Reson Imaging*. 2017;45:1154–1162.
42. Busse H, Kahn T, Moche M. Techniques for interventional MRI guidance in closed-bore systems. *Top Magn Reson Imaging*. 2018;27:9–18.
43. Fritz J, Pereira PL. MR-guided pain therapy: principles and clinical applications [in German]. *Rofo*. 2007;179:914–924.
44. Baker KB, Tkach JA, Nyenhuis JA, et al. Evaluation of specific absorption rate as a dosimeter of MRI-related implant heating. *J Magn Reson Imaging*. 2004;20:315–320.
45. Baltzer PAT, Bickel H, Spick C, et al. Potential of noncontrast magnetic resonance imaging with diffusion-weighted imaging in characterization of breast lesions: intraindividual comparison with dynamic contrast-enhanced magnetic resonance imaging. *Invest Radiol*. 2018;53:229–235.
46. Pinker K, Moy L, Sutton EJ, et al. Diffusion-weighted imaging with apparent diffusion coefficient mapping for breast cancer detection as a stand-alone parameter: comparison with dynamic contrast-enhanced and multiparametric magnetic resonance imaging. *Invest Radiol*. 2018;53:587–595.
47. Frahm J, Voit D, Uecker M. Real-time magnetic resonance imaging: radial gradient-echo sequences with nonlinear inverse reconstruction. *Invest Radiol*. 2019;54:757–766.
48. Runge VM, Richter JK, Heverhagen JT. Motion in magnetic resonance: new paradigms for improved clinical diagnosis. *Invest Radiol*. 2019;54:383–395.
49. Fritz J, Fritz B, Zhang J, et al. Simultaneous multi-slice accelerated turbo spin echo MRI: comparison and combination with in-plane parallel imaging acceleration for high resolution MRI of the knee. *Invest Radiol*. 2017;52:529–537.